



## Regular Article

## On the measurement and scaling of mixing time in orbitally shaken bioreactors

G. Rodriguez<sup>a</sup>, T. Anderlei<sup>b</sup>, M. Micheletti<sup>a</sup>, M. Yianneskis<sup>c</sup>, A. Ducci<sup>c,\*</sup><sup>a</sup> University College London, Department of Biochemical Engineering, Torrington Place, London, WC1E 7JE, UK<sup>b</sup> Adolf Kühner AG, Dinkelbergstrasse 1, CH-4127 Birsfelden, Switzerland<sup>c</sup> University College London, Department of Mechanical Engineering, Torrington Place, London, WC1E 7JE, UK

## ARTICLE INFO

## Article history:

Received 17 June 2013

Received in revised form 24 October 2013

Accepted 27 October 2013

Available online 4 November 2013

## Keywords:

Shaken bioreactor

Orbital shaking

Mixing time

Mixing

Dual indicator method

Scaling

## ABSTRACT

Accurate determination of the mixing time in orbitally shaken bioreactors (OSRs) is essential for the optimization of mixing processes and minimization of concentration gradients that can be deleterious to cell cultures. The Dual Indicator System for Mixing Time (DISMT) was employed to measure mixing times in cylindrical and Erlenmeyer flask bioreactors. Various aspects of importance for the acquisition of accurate data from the measurement methodology are discussed, utilizing also comparisons of DISMT and pH probe results obtained in two stirred reactors. The OSR results are juxtaposed with data previously reported in the literature for both cylindrical reactors and Erlenmeyer flasks. The employment of a critical Froude number shows promise for the establishment of a scaling law for mixing time across the various types and sizes of shaken bioreactors.

© 2013 Elsevier B.V. All rights reserved.

## 1. Introduction

Mammalian cell cultures have been widely used for the production of therapeutic proteins and vaccines. Monoclonal antibodies, in particular, represent a class of therapeutics that has shifted the treatment paradigm in the fields of oncology and immunology by improving the quality of life for the patient during cancer treatment [1,2]. Commercial production of these antibodies relies on the development of cost-effective large-scale cultivation methods of genetically engineered mammalian cells. At laboratory scale, cells are usually grown in low shear devices, with orbitally shaken bioreactors (OSRs) being largely employed in the early stages of bioprocess development because they offer an effective solution to screen several conditions in parallel. This low energy demand and the well-defined gas–liquid interface, make orbitally shaken bioreactors a favourable solution that provides a promising environment for mammalian cell cultivation in terms of oxygen transfer

and nutrient requirements. Once the process is optimized at small scale, it is then adapted to stirred tank reactors (STRs), which is the type of bioreactor most commonly used at production level. STRs have been thoroughly characterized in the literature (for example, [3–6]).

The differences between the mixing mechanisms occurring at the two scales and geometries represent a challenge for scale-up to commercial manufacture. Such differences may result in inadequate mass transfer characteristics, cell damage and reduced antibody productivity. Studies of animal cell cultures have focused on optimizing the chemical environment and culture media in order to enhance antibody productivity [7,8], but studies of the engineering characteristics relevant to the optimization of bioreactor geometry and operating conditions are still lacking. While growth rates in mammalian cell cultures are slower than those in microbial systems, the need for a well-mixed environment has been acknowledged in terms of the quality of cell suspension and gas supply and removal [9–12]. Recent studies in STRs have shown that shear stresses do not significantly affect cell growth of animal cells [13,14], however there is a growing interest in understanding the effect of shear stress on stem cells and cells for therapy, and the low shear levels present in OSRs could potentially make this device a suitable option for scaling up cell expansion using suspension cultures [15]. From this point of view operating conditions should be carefully selected by comparing the Kolmogorov length scale to

*Abbreviations:* OSR, orbital shaken reactor; STR, stirred tank reactor; 2D, two-dimensional; 3D, three-dimensional; CFD, computational fluid dynamics; PIV, particle image velocimetry; DISMT, Dual Indicator System for Mixing Time; RGB, red green blue colour model; HSV, hue saturation value colour model.

\* Corresponding author. Tel.: +44 2076797397.

E-mail address: [a.ducci@ucl.ac.uk](mailto:a.ducci@ucl.ac.uk) (A. Ducci).

$a_o$	constant
$d_i$	inner diameter of the cylinder (m)
$d_o$	orbital or shaking diameter (m)
$d_b$	Erlenmeyer bottom diameter (m)
$Fr$	Froude number
$Fr_{d_i}$	Froude number based on the inner diameter of the cylinder
$Fr_{d_o}$	Froude number based on the orbital diameter
$G_{i,j}^*$	normalized intensity of the green channel in the $i$ th $j$ th pixel
$g$	gravitational acceleration ( $\text{m s}^{-2}$ )
$H$	cylinder height (m)
$h$	fluid height (m)
$\Delta h$	free surface height (m)
$I_a$	free surface interfacial area ( $\text{m}^2$ )
$M$	global degree of mixing
$N$	shaker table rotational speed ( $\text{s}^{-1}$ )
$N_{cr}$	critical shaker table rotational speed ( $\text{s}^{-1}$ )
$Re$	Reynolds number
$T_\theta$	circulation time around the toroidal vortex axis (s)
$T_z$	circulation time around the cylinder axis (s)
$t_{95\%}, t_m$	mixing time (s)
$V$	nominal volume ( $\text{m}^3$ )
$V_L$	liquid/filling volume ( $\text{m}^3$ )
$X$	local degree of mixedness

#### Greek symbols

$\theta$	mixing number
$\varphi$	phase angle of the table ( $^\circ$ )
$\sigma_G$	standard deviation of the normalized green channel across the field of view at time $t$

the size of the microcarriers or cell aggregates [16]. The intrinsic differences between stirred vessels and orbitally shaken bioreactors have motivated the development of production scale OSRs [17,18] and industrial efforts to provide a single piece of equipment for different cell culture processes at multiple scales. Despite recent progress of shaken bioreactor platforms, with the development of optical sensors and control loops to improve automation in millilitre scale bioreactors, the number of publications which address scaling up/down aspects of shaken bioreactors is very limited [19].

#### 1.1. Flow characterization and transition in orbitally shaken bioreactors

Gardner and Tatterson [20] were the first to report the flow and mixing dynamics in a shaken cylindrical vessel. Dye visualization techniques with mixtures of different viscosity were employed to assess the variation of the homogenization time with increasing Reynolds number,  $Re$ . Büchs et al. [21] estimated the power consumption in Erlenmeyer flasks by measuring the torque on the drive acting upon the shaker table and taking into account friction and other system losses. The effects of size of the container, filling volume, shaking or orbital diameter, shaking frequency and liquid viscosity were investigated. At certain agitation regimes an 'out-of-phase' condition occurred, when the liquid in the shaken flask did not move in synchronization with the shaker table. Klöckner et al. [22] extended the work of [21] to estimate the power consumption of cylindrical shaken bioreactors. Contrary to the results obtained for Erlenmeyer flasks, the orbital to internal diameter ratio  $d_o/d_i$  was found to affect the power number. The correlation of Eq. (1) was proposed to estimate the critical shaking speed,  $N_{cr}$ , which for cylindrical OSRs may be used to identify 'suitable' shaking

conditions associated with a measurable power number and in-phase flow.

$$N_{cr} = \frac{1}{d_i^2} \sqrt{0.28Vg} \quad (1)$$

The study of Weheliye et al. [23] was the first to provide a thorough insight into the dynamics of the flow occurring inside a cylindrical shaken bioreactor, and to determine a flow scaling law based on physical considerations, without resorting to the use of power law correlations. The work covered different internal diameters, filling volumes, orbital diameters, and agitation speeds and made use of phase-resolved particle image velocimetry (PIV) and free surface measurements. The scaling law was formulated based on the consideration that the free surface orientation,  $\Delta h/d_i$ , is orthogonal to the resultant force obtained from the vectorial sum of the centrifugal force due to the orbital motion and the gravitational one (see Eq. (2)).

$$\frac{\Delta h}{d_i} = a_o \left( \frac{2(\pi N)^2 d_o}{g} \right) \quad (2)$$

where  $\Delta h$  is the maximum height difference between diametrically opposite points on the free surface, and is hereafter denoted as the wave amplitude induced by the orbital motion. The constant of proportionality,  $a_o$ , depended on the fluid considered. The relationship of Eq. (2) was tested for several combinations of non-dimensional fluid height,  $h/d_i = 0.3\text{--}0.7$ , and orbital to cylinder diameter ratio  $d_o/d_i = 0.14\text{--}0.5$ . The measured data and the correlation of Eq. (2) showed very good agreement at low speed or Froude number  $Fr$ . At greater  $Fr$  the free surface exhibited a complex three-dimensional shape, which is due to local non-uniformities of the inertial to the gravitational force ratio, and its mean inclination started deviating from the linear relationship of Eq. (2). Weheliye et al. [23] showed that the variation of free surface shape corresponded to the onset of a flow transition from a horizontal toroidal vortex to a vertical one processing around the cylinder axis, before and after the transition, respectively. This flow transition is determined by the growth in size of the toroidal vortex with increasing rotational speed,  $N$  (i.e.  $Fr$ ), and it occurs when the toroidal vortex extends over the entire fluid height. They concluded that the flow transition in a shaken cylindrical bioreactor can be predicted using either Eq. (3) or (4) depending whether  $h/d_i < (d_o/d_i)^{0.5}$  or  $h/d_i > (d_o/d_i)^{0.5}$ , respectively.

$$\frac{h}{d_i} = a_o \left( \frac{d_i}{d_o} \right)^{0.5} Fr_{d_o} \quad (3)$$

$$a_o Fr_{d_i} = 1 \quad (4)$$

where the Froude numbers  $Fr_{d_o}$  and  $Fr_{d_i}$  are estimated from Eq. (5) using the orbital and cylinder diameters, respectively.

$$Fr = \frac{2\pi^2 N^2 d}{g} \quad (5)$$

Given the broad range of definitions of Froude number available in literature, the definition of Eq. (5) was selected for consistency with the works of [21,23–25].

#### 1.2. Mixing time in bioreactors

Macro-mixing time studies based on a colorimetric method have been carried by Tissot et al. [26] and Tan et al. [27] in shaken cylinders and flasks, respectively. This approach has been widely used in stirred tanks, employing either a single or a combination of two pH indicators, and it has been thoroughly analyzed by Cabaret et al. [28] to optimize both the experimental and post-processing aspects of the colorimetric methodology. Tissot et al. [26] used a

Dual Indicator System for Mixing Time (DISMT) to estimate from visual observations the variation of mixing time in shaken cylinders of different nominal volumes with shaken speed,  $N$ , cylinder diameter,  $d_i$ , orbital diameter,  $d_o$ , and fluid height,  $h$ . Their study showed the presence of different regions within the tank characterized by very different mixing dynamics: a slow mixing zone close to the cylinder bottom, where mixing was mainly determined by diffusion, and a region closer to the cylinder wall, where the high shear rates induced fastest mixing. Mixing times were found to be inversely proportional to Froude numbers, defined in that study as  $Fr = \pi N(d_o + d_i)/\sqrt{gd_i}$ , while a reduction in cylinder diameter,  $d_i$ , resulted in an increase of mixing times at constant  $N$ . Based on these considerations and the experiments they carried out in small ( $V=30$  l), and large ( $V=1500$  l) scale bioreactors, they empirically derived the correlation of Eq. (6) to scale the mixing number,  $\theta$ .

$$\theta = Nt_m \left( \frac{\delta_{o,30\text{ l}}}{\delta_{o,1500\text{ l}}} \right) \quad (6)$$

where  $\delta_{o,30\text{ l}}$  and  $\delta_{o,1500\text{ l}}$  are the orbital diameters for the 30 l and 1500 l bioreactors, respectively.

Tan et al. [27] employed a single indicator system to determine through visual inspection the mixing in an unbaffled Erlenmeyer shaken flask. They reported that mixing times obtained with a colorimetric method are only indicative of the time required to achieve colour uniformity within the tank upon reaching a preselected pH threshold, as this does not necessarily imply pH homogeneity, which is achieved only when the diffusion process is complete. Therefore comparison with mixing times obtained with other techniques should be made with care. Taking this into account, Tan et al. [27] showed by means of a log–log plot that mixing times in shaken flasks exhibit a similar trend to those obtained in stirred tank reactors with different types of impellers, with a decrease of mixing number with increasing  $Re$ . In contrast to the study of [26] for a shaken cylinder, Tan et al. [27] concluded that the shaking diameter  $d_o$  has no significant effect on the mixing time in unbaffled Erlenmeyer flasks. However it should be noted that the reported agreement between the mixing times obtained for  $d_o = 25$  mm and 50 mm vessels was obtained with a tolerance of  $\pm 30\%$ .

Mixing time measurements by Rodriguez et al. [29] provided point-by-point quantification of the mixing time distribution in an OSR obtained from mixing maps constructed from DISMT data, and the first attempt to provide an objective and reproducible procedure based on syringe pump insertion, fixed feed volume and image processing routines to determine the mixing time in OSRs. They showed that the mixing number may be affected by the position of the feeding pipe. This occurred mostly for feeding positions close to the centre of the bioreactor, for which the probability of insertion into either the toroidal or axial vortices (i.e. for conditions before or after transition to out-of-phase flow) resulted in an entrainment of the inserted volume into the vortex. Their data indicated that insertion should be made closer to the wall where shear stresses induced by the boundary layers enhance the dispersion and deformation of the inserted initial blob and therefore the mixing in the bioreactor. Selection of positions closer to the wall was also advised at the higher  $Fr$  regime after flow transition, when turbulence starts to emanate from the boundary layers at the side walls. Counter-intuitively, material entrained and trapped inside the vortex may mix more slowly, even with a greater mean circulation provided by a higher orbital speed. This work highlighted the need for care in mixing time experiments in OSRs as the longer mixing times resulting from insertion inside the vortex contrast sharply with results in STRs where in-vortex insertion can result in a reduction of mixing time by 25–30% [30,31], as the feed is drawn directly towards the impeller, where it is broken up and dispersed more quickly.

The research reported in this paper builds upon the studies of [23,29] and the aim of the present work is twofold. First, aspects of the DISMT methodology of importance for the improved interpretation and reliability of the acquired data are identified and discussed. Second, through juxtaposition of the present data with those previously reported for other reactor shapes and sizes, an attempt is made to establish a scaling law for mixing time that shows promise for comparison of the mixing achieved in different reactor geometries.

## 2. Materials and methods

### 2.1. Bioreactor geometries

Mixing time measurements were obtained in a total of seven reactors, five OSRs and two STRs. The latter were employed to assess DISMT pH data against those obtained with pH probes.

The first STR was a single use 3L Mobius® CellReady shown in Fig. 1(a). The bioreactor consists of an unbaffled 137 mm diameter plastic tank with a height to diameter ratio of 1.8:1. The CellReady maximum and minimum working volumes are 2.4 l and 1 l, respectively. It is agitated by a 3 blade, up-pumping marine impeller 76.2 mm in diameter positioned on a centre shaft 28 mm from the tank bottom [32]. In the present experiments filling volumes of 1 l and 2 l were used and the impeller speed range was 100–200 rpm. The second STR was a New Brunswick BioFlo 110 5.5 l glass vessel with a dome base and removable baffles, where agitation is accomplished with two 6-bladed Rushton impellers with a diameter of 58 mm and clearance from the bottom of 65 mm and 125 mm (see Fig. 1(b)). The vessel diameter and height are 190 mm and 290 mm, respectively, and experiments were carried out with a filling volume  $V=4.5$  l for a rotational speed  $N=50$  rpm.

Three of the OSRs were of cylindrical shape and two were Erlenmeyer flasks. The first cylindrical reactor (Fig. 1(c)) comprised a glass cylinder with a transparent bottom placed in a square acrylic trough to minimize refraction. A steel structure enclosed the trough and cylinder, leaving the top of the cylinder open. The cylinder inner diameter,  $d_i$ , height,  $H$ , and wall thickness,  $t_c$ , were 100 mm, 250 mm and 5 mm, respectively. Filling volumes of 235, 393 and 550 ml were used, corresponding to  $h$  of 30, 50 and 70 mm, respectively. The second and third cylindrical reactors investigated comprised the same geometry as in Fig. 1(c), but with  $d_i$  of 70 mm and 130 mm, respectively. The fluid height to diameter ratio  $h/d_i$  was kept constant, resulting in  $h=35$  mm for the  $d_i=70$  mm cylinder and  $h=65$  mm for the  $d_i=130$  mm cylinder and corresponding volumes of 134 ml and 862 ml. The shaker rotational speed was varied in the range  $N=90$ –210 rpm, and the orbital diameter was  $d_o=25$  mm for all such experiments.

The two Erlenmeyer flasks had nominal working volumes of 1 l and 2 l and the corresponding filling volumes were 400 ml and 800 ml. Experiments were made over the speed range 100–200 rpm. The geometrical and operating parameters of the vessels used in this work are summarized in Table 1.

### 2.2. Dual Indicator System For Mixing Time

The Dual Indicator System for Mixing Time (DISMT) first developed by Melton et al. [33] was employed for the mixing time measurements. DISMT comprises a fast acid–base reaction between sodium hydroxide (NaOH) and hydrochloric acid (HCl) in the presence of two pH indicators, Methyl Red and Thymol Blue. The Methyl Red indicator turns from red to yellow in the pH interval 4.2–6 and Thymol Blue turns from yellow to blue in the pH interval 8.0–9.6. The combination of such pH indicators results in the fluid being red for  $\text{pH} < 6$ , blue for  $\text{pH} > 8$  and yellow for  $6 < \text{pH} < 8$ .

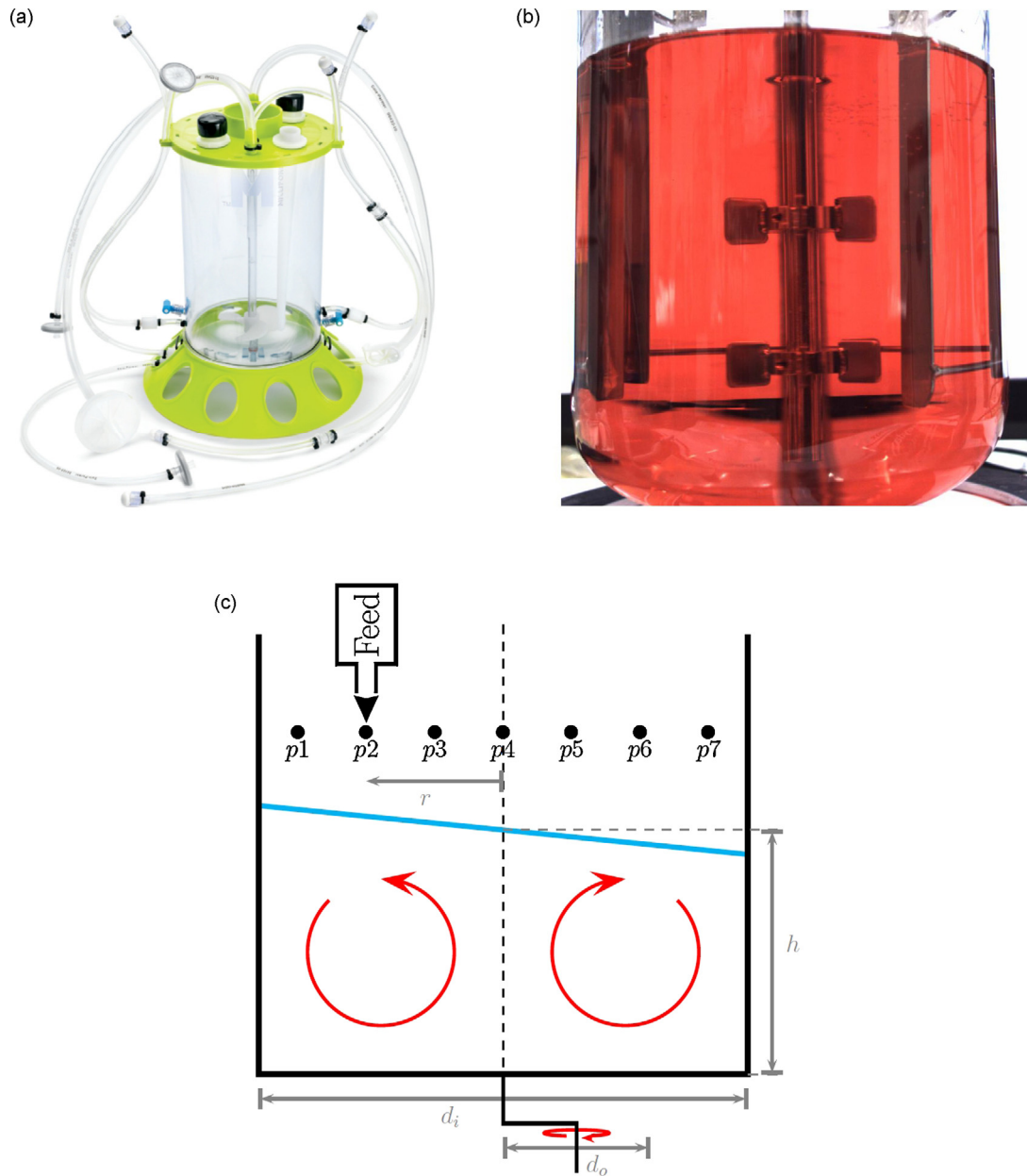


**Fig. 1.** (a) Picture of the Mobius® CellReady reactor; (b) picture of the BioFlow stirred reactor; (c) sketch of the cross-sectional view of the orbitally shaken cylindrical bioreactor and of the feed pipe locations.

The indicators were prepared in a volume of de-ionized water at a final concentration of 4.3 mg/l. This allowed to mimic typical media solutions used in mammalian cell cultures which have water-like viscosities [26]. The fast acid-base reaction is initiated by inserting stoichiometric amounts of base (sodium hydroxide) in a solution containing Type 2 pure Lab Water (ASTM D1193) and

the pH indicators, previously acidified with 0.5 ml/l of Hydrochloric Acid at a concentration of 0.5 M. At the beginning of the experiment the solution in the vessel concerned was acidic (red). The base was inserted after the shaker table had completed at least three revolutions and the flow inside the bioreactor was fully developed.

**Table 1**

List of the different experimental conditions investigated with DIMST in orbitally shaken reactors.

Geometry	Reactor diameter [mm]	Orbital diameter, $d_o$ [mm]	Fluid height, $h$ [mm]	Fill, nominal volumes [l]	Speed range, $N$ [rpm]
Cylinder	$d_i = 70$	25	35	0.538	110–200
	$d_i = 100$		30	0.942	140–210
			50	1.5	100–200
			70	2.2	90–210
			75	3.98	90–200
Erlenmeyer flask	$d_b = 131$	25	–	0.4, 1	100–200
	$d_b = 166$		–	0.8, 2	100–200

In the 70, 100 and 130 mm cylindrical OSRs, mixing time experiments were carried out with the feeding pipe being located on the open end of the glass cylinder, at the radial position  $r/d_i = 0.3$ , denoted as P3 in Fig. 1(c). To reduce the statistical error each set of experiments comprised 20 repetitions and the averaged mixing time from these 20 tests was estimated. The feeding pipe was constructed with microfluidics connectors (IDEX Health and Science) and was fed by a Harvard Apparatus syringe pump. The vessel was positioned on a Kühner AG LS-X lab shaker equipped with a 360° encoder. A colour NET iCube camera was fixed to the shaker table to record the experiments. To reduce background noise an 8 LED OMC backlight panel with a homogeneous 580 mcd white light source was positioned at the back of the experimental rig and rotated rigidly with the shaker table. The shaker table encoder and timing box allowed complete synchronization of the motion of the table, the camera and the syringe pump insertion. The feed insertion was always made when the shaker table was at its position furthest to the left and it was nearly instantaneous, lasting around 2 ms (i.e. over an angle of rotation  $\Delta\varphi < 2.5^\circ$  for every rotational speed considered). Phase-locked images were recorded at every revolution for a phase angle  $\varphi = 0^\circ$ , which corresponds to the orbital point furthest to the left when the system is viewed from the top. Phase-locked measurements allowed to “freeze” the free surface motion at its maximum inclination position, resulting in a significant simplification of the image post-processing routines that did not have to take into account the cyclic variation of the fluid distribution inside the tank.

The same experimental procedure was used to perform mixing time measurements in two DIN ISO 24450 wide mouth Erlenmeyer flasks of nominal volume  $V = 1$  l and 2 l, with flask bottom diameters of 131 mm and 166 mm, respectively. Experiments were carried out with an orbital diameter  $d_o = 2.5$  cm, and agitation rates  $N = 100$ –200 rpm. For this set of experiments the base feed was inserted manually with a hand pipette, while, to have consistent experiments to those carried out in orbitally shaken cylinders, the fill to nominal volume ratio was kept constant at 40%, close to the 30% ratio typically used for this flask. It is worth to remark that this ratio is higher than those generally used in practical applications, and for example in the study of [27] the fill and nominal volumes were 50 ml and 500 ml, respectively, with a volume ratio of 10%.

For the CellReady and New Brunswick BioFlo STRs the DIMST technique previously described was used concurrently with measurements taken by pH probes built into the bioreactors. This allowed to further validate the mixing time estimates obtained from the colorimetric methodology. In the New Brunswick BioFlo pH readings were acquired every 12 s by the BioFlo controller connected to a Hamilton Easyferm plus k8325 probe, while the data acquisition rate of the pH probe of the cell ready bioreactor was 1 Hz. The two off-the-shelf STRs were not equipped with an encoder, and, as a consequence, phase-resolved DIMST measurements could not be carried out as for the OSRs. For these sets of experiments the iCube camera was triggered at a constant frequency of 4 Hz, which is fast enough to capture the macro-mixing dynamics of the bioreactors, and the pH measurements were started concurrently with the image acquisition at the instant of base addition. In the CellReady bioreactor, addition of a stoichiometric amount of NaOH was performed at the free surface using a port on the top cover at a radial position 50 mm from the impeller axis using the microfluidics connectors and syringe pump. Two fill volumes were investigated: 1 l and 2 l at agitation rates at 150 rpm ( $Re = 14,000$ , turbulent flow regime). In the new Brunswick BioFlo experiments were performed with  $V = 4.5$  l and  $N = 50$  rpm ( $Re = 2000$ , transitional flow regime). It should be stressed that measurements in the CellReady and New Brunswick BioFlo STRs were made solely to assess

the applicability of the DIMST technique to this type of reactors.

### 3. Results and discussion

#### 3.1. Appraisal of different methodologies for the determination of mixing time

Mixing time measurements obtained from colorimetric and decolourization methods are often made visually by an operator inspecting the experiment in real-time or a recorded video (see, for example, [11,27]). This approach has an inherent degree of subjectivity, which inevitably increases the error made on mixing time estimates, especially when large datasets are processed, and significantly limits the reproducibility/comparability of the data in/between different laboratories. In the current study image processing routines were developed to get objective mixing time estimates and, as suggested by [28], mixing condition maps were built to identify and quantify zones in the bioreactor where mixing is poor.

The time evolution of the mixing time experiments indicates a colour change from red to yellow, with local concentrations of blue hues in the transient. The iCube camera acquired images in RGB format, and therefore the colour variation in each pixel is a combination of the intensities of the red, green and blue channels.

The analysis of colour video images is a rather complex process that necessitates careful selection of the image processing methodology to ascertain the colour (and, for the present application, the pH) exhibited by each pixel on an image. A detailed description of the intricacies and potential pitfalls of colour measurement (in relation to the analysis of images of thermochromic liquid crystals) is provided by [34]. In brief, colour may be apportioned to a pixel directly from the red, green and blue outputs of a camera (RGB), or via the hue, saturation and value (HSV) 3D colour space representation that is derived from the RGB values. In effect, hue refers to the perceived colour, saturation to the amount of colour and value to the brightness of each element of the analyzed image.

A characteristic variation in time of the three RGB channels is given in Fig. 2(a) for a location ( $r/d_i = 0.375$ ,  $z/d_i = 0.25$ ) on the right side of the  $d_i = 100$  mm cylindrical bioreactor as shown in the inset of Fig. 3(a). In the abscissa the time is indicated by  $Nt$ , i.e. the number of shaker table revolutions from the start of the mixing process. The blue channel output varied the least, by around 50, while both the red and green channels showed maximum variations of around 150 and 200, respectively, out of a maximum value of 254. On average, the time evolution of the green channel exhibited a sigmoidal shape, consistent with the colour change from red to yellow induced by the base insertion, while the red channel exhibited a U-shape indicating that a high level of red is also present in the final yellow hue achieved at the end of an experiment. Similar time variations to those shown in Fig. 2(a) were exhibited by all three channels at all other points in the flow.

The variation of the HSV values with time at the same location as in Fig. 2(a) is shown in Fig. 2(b). As with the RGB data, similar HSV variations to those in Fig. 2(b) were recorded at all other points in the flow. Although the  $V$  values exhibit the largest variation with time, it is the hue that is representative of colour but it exhibits a far smaller variation. Consequently, the RGB data were preferred for the extraction of colour change information. To reduce the computational cost of the data-processing, and in agreement with the previous mixing time experiments of [26,28], only the green channel was selected to measure the mixing time because it exhibited the least amount of background noise in comparison to the total intensity variation between the start and the end of the experiment. From this point of view it is clear that a composite index, made up

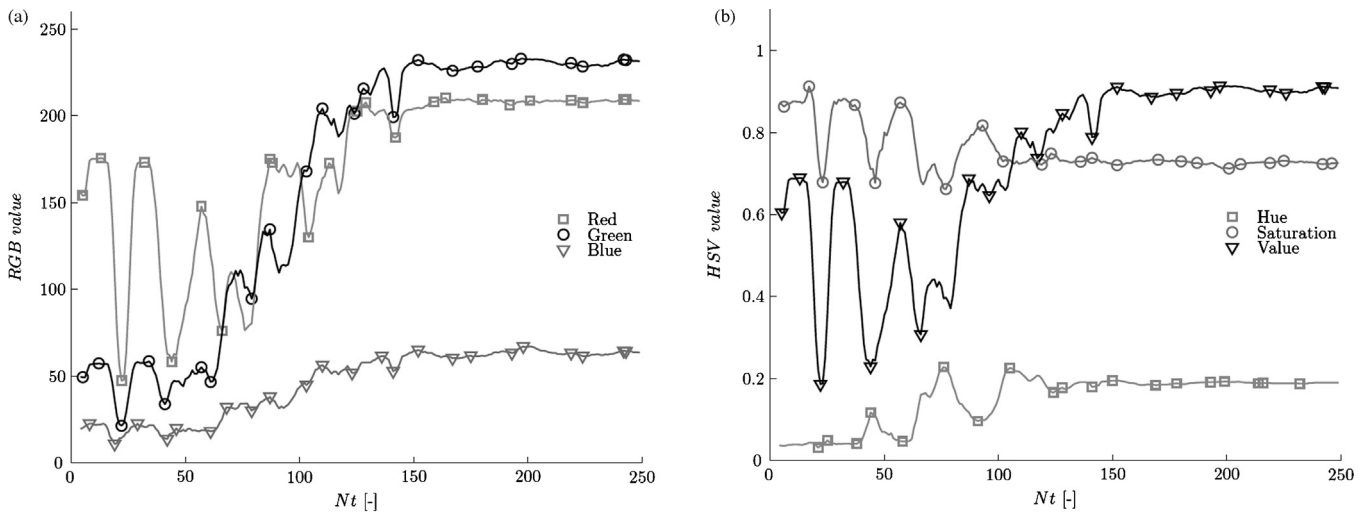


Fig. 2. Variation with orbital revolutions,  $Nt$ , of the three channels in the RGB (a), and in the HSV representation of colour (b) ( $r/d_i = 0.375$ ,  $z/d_i = 0.25$ ).

of different percentages of the red, blue and green channels, would have been less effective at determining the colour variation than the green channel alone. This can be better understood when thinking at the extreme case of a grey scale space representation, where all channels are weighted the same. The use of the blue and red channels would have dampened the greater variation associated to the green channel, resulting in a less effective composite index.

It should be noted that the depth-of-field of the colour image in the three-dimensional reactor that is recorded by the two-dimensional camera sensor varies with radial coordinate or

distance from the centre of the vessel. Consequently, it should be determined to what extent the colour recorded at different radial coordinates was influenced by this effect. For example the intensity of the colour in a point on the axis of the cylinder,  $r/d_i = 0$ , is determined by a horizontal volume of fluid which has a depth equal to the diameter of the cylinder. On the other hand, when considering points closer to the cylinder walls, at  $r/d_i = 0.5$ , the depth of the fluid orthogonal to the camera field of view tends to zero at near-wall positions and the colour intensity decreases. This colour variation and the associated steady state inhomogeneity across the field of view introduce a systematic error in the final mixing time estimate. To eliminate this uncertainty, the green intensity level of each pixel was normalized according to Eq. (7):

$$G_{i,j}^* = \frac{G_{i,j}(t) - G_{i,j}(t_0)}{G_{i,j}(t_\infty) - G_{i,j}(t_0)} \quad (7)$$

The indices  $i$  and  $j$  denote a pixel in the field of view and  $G_{i,j}(t)$ ,  $G_{i,j}(t_0)$  and  $G_{i,j}(t_\infty)$  are the pixel green intensity at time  $t$ , at the start and at the end of the experiment, respectively. The steady-state (fully-mixed condition) green intensity  $G_{i,j}(t_\infty)$  is obtained from the average of the last five data points on the time evolution curve. With this normalization procedure all pixels have the same  $G_{i,j}^*$  intensity at the beginning ( $G_{i,j}^* = 0$ ) and at the end ( $G_{i,j}^* \approx 1$ ) of an experiment. Meeting these two conditions is essential for  $G_{i,j}^*$  to reflect the homogeneity of the fluid both before the base insertion and at the fully-mixed state.

A characteristic variation of the normalized green,  $G_{i,j}^*$ , and red,  $R_{i,j}^*$ , channels, with time, for the same point in the flow as in Fig. 2, is presented in Fig. 3(a). The position of the measurement point is at the centre of the area delimited by the white box in the inset in the figure. From Fig. 3(a) it is evident that after normalization both channels satisfy the two conditions,  $G_{i,j}^*(0) = 0$ ;  $G_{i,j}^*(\infty) \approx 1$ , previously outlined. It is interesting to note that the variation of the normalized green and red channels data exhibits fluctuations, which, as expected, are similar to those of the non-normalized channels represented in Fig. 2(a) and (b), but those of the red channel are greater in amplitude, and therefore  $R_{i,j}^*$  represent a more meaningful parameter to study the mixing transient. These fluctuations are quasi-periodical for the first part of the trace, with a period of around 20 revolutions. These fluctuations stem from the movement of the reactants in the vessel and reflect the large changes of colour and pH that may be encountered at a point during the mixing process. The 10 triangular symbols in both curves of Fig. 3(a)

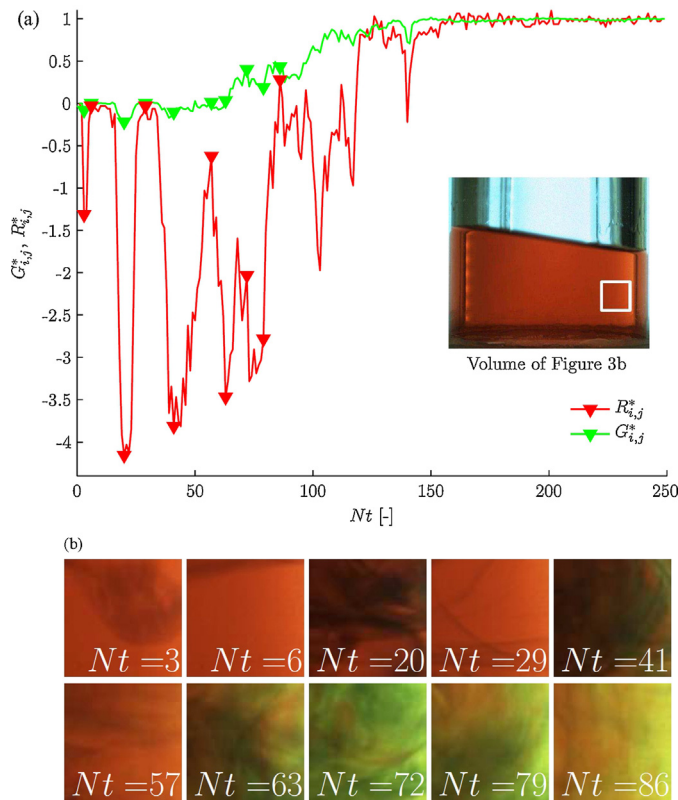


Fig. 3. (a) Variation in time of the normalized green index,  $G_{i,j}^*$ , for the point of the bioreactor at the centre of the area delimited in the inset image; (b) colour evolution in time within the area highlighted in the inset image of (a).

correspond to the 10 volume snapshots shown in Fig. 3(b). The aforementioned large colour/pH variations can be clearly seen in Fig. 3(b); the predominance of dark brown colour (i.e. high  $B_{i,j}^*$ , and comparatively low  $R_{i,j}^*$  and  $G_{i,j}^*$ ) at  $Nt = 20, 41$  and  $63$  corresponds to the fluctuation frequency mentioned above.

An assessment of this frequency was made from the circulation times estimated from the PIV measurements of [23] for similar flow conditions. Figs. 2 and 3 were obtained for incipient out-of-phase flow ( $N = 90$  rpm;  $d_o = 2.5$  cm,  $d_i = 100$  mm,  $h = 5$  cm), when the toroidal vortex extends to the bottom of the tank. From the ensemble-averaged data of [23] the circulation time required for a fluid parcel to complete a loop around the toroidal vortex axis is estimated as approximately 1.67 shaker table revolutions. Similarly an estimate of 4 revolutions around the toroidal vortex axis (oriented along the azimuthal direction) is obtained for a fluid parcel to complete a loop around the cylinder axis (oriented in the vertical direction). Consequently, a parcel will proceed along a spiral path for  $4 \times 1.67 = 6.68$  shaker table revolutions, before occupying again its initial position in the cylinder. The mixing time maps of Fig. 3(b) were obtained from phase-resolved DIMST data that are under-sampled, capturing only 1 of every 3 periods of the parcel motion (as  $3 \times 6.68 = 20$ ). It should be stressed that this analysis is approximate and any conclusions should be drawn with care, as a fluid parcel trajectory is being extrapolated from ensemble-averaged results. Nevertheless the present data provides the first explanation of the periodicity observed and indicates that further experiments, with more advanced methodologies such as laser induced fluorescence, should be carried out to further investigate such advection characteristics in the bioreactor and provide measurements of the circulation time.

The selection of mixing criteria to estimate the final mixing time is important in order to obtain objective and reliable estimates. From this point of view the detailed analysis of the post processing of colorimetric data by [28] in a stirred reactor distinguished between two main mixing thresholds: a local degree of mixedness,  $X$ , that is achieved in a single pixel when the condition  $G_{i,j}^*(t) > X$  is met, and a global degree of mixedness,  $M$ , that represents the percentage of pixels that must achieve local mixing for the entire reactor to be considered as fully mixed. In their study Cabaret et al. [28] built a mixing map ( $X, M$ ) to establish whether an optimum range of the two thresholds exists to minimize the error made in the final mixing time. Their study highlighted that curves displaying the evolution in time of the global mixing index,

$M$ , against the local mixing threshold  $X$  selected were characterized by an inflection with nearly constant  $M = 70\%$  for values of  $X$  in the range of 40–60%. This meant that in this range the final value of mixing time was less sensitive to small variations in  $M$  and  $X$ . A similar analysis was carried out in the present study, and the resulting variation in time of  $M$ - $X$  curves for a mixing time experiment in the Mobius® CellReady reactor, with a fill volume of 2 l agitated at 150 rpm, is shown in Fig. 4. The present data show an opposite behaviour to that reported in [28], as in Fig. 4 an inflection point occurs with nearly constant  $X = 70\%$  for values of  $M$  in the range of 40–60%. The reason for this difference can be explained by considering that Cabaret et al. [28] used a highly viscous fluid, which determined the formation of segregated regions in proximity of the impeller, where pockets of fluid with more base or acid concentrations were entrained in the vortex loops present above and below the turbine. This meant that in their case the percentage of the tank volume considered,  $M$ , affects to a greater extent the final mixing time for a given experiment, and, for example, lower mixing time values would be achieved if the analysis was restricted to the segregated regions. On the contrary, in the present case a water solution was used as working fluid, and therefore mixing dynamics are faster across the tank, and the final mixing time estimate is affected to a greater extent by the local mixing threshold selected, rather than by the size of the volume investigated. From the results of Fig. 4 and related data across the vessel, the condition for which both  $M$  and  $X$  were 95%, indicated by an asterisk in the figure, was considered for completed mixing in the present work. Correspondingly, the mixing time used for the results hereafter is denoted as  $t_{95\%}$ , when 95% of the final value has been reached.

Two different approaches were adapted to determine the mixing time,  $t_{95\%}$ . One involved estimating the standard deviation of  $G_{i,j}^*$  across the field of view at each instant, and considering that the fully mixed condition was achieved when the standard deviation was below a selected threshold. A typical variation of the standard deviation,  $\sigma_G$ , with the number of bioreactor revolutions,  $Nt$ , is shown in Fig. 5(a). The standard deviation is zero at the start of the mixing process and rises sharply once the feed base is inserted. Subsequently, at high values of  $t$  the standard deviation tends towards a constant value of around 0.03. The mixing time is then estimated, for both this and the second method described below, as the average of the times necessary to achieve 13 different degrees of homogeneity, from 92% to 98%, with respect to the steady state value, from Eq. (8). This methodology was implemented by Micheletti et al. [35] as it facilitates the minimization of scatter in the mixing time data due to signal noise. For example the time shown in Fig. 5(a) (63 revolutions) is that required for 95% of the final value of  $\sigma_G$  to be achieved.

$$t_{95\%} = \sum_{i=1}^{13} \frac{t_{i\%}}{13} \quad (8)$$

The second method employed to determine the mixing time made use of the percentage of pixels,  $M$ , that have achieved the degree of mixing as indicated in Eq. (9).

$$|G_{i,j}^* - 1| < 0.05 \quad (9)$$

The mixing time in this case is provided by the number of revolutions for which 95% of the pixels are mixed ( $M = 95\%$ ). The variation of  $M$  with  $Nt$  is also shown in Fig. 5(a) for the same operating conditions,  $Fr_{d_o} = 0.24$  and  $h/d_i = 0.5$ . The  $M$  curve is of sigmoid shape. An abrupt rise is observed after around 50 revolutions and the mixing is completed after 58 revolutions. The 8% difference between the mixing times yielded by the two approaches highlights the sensitivity of the results to the methodology adopted and shows that care

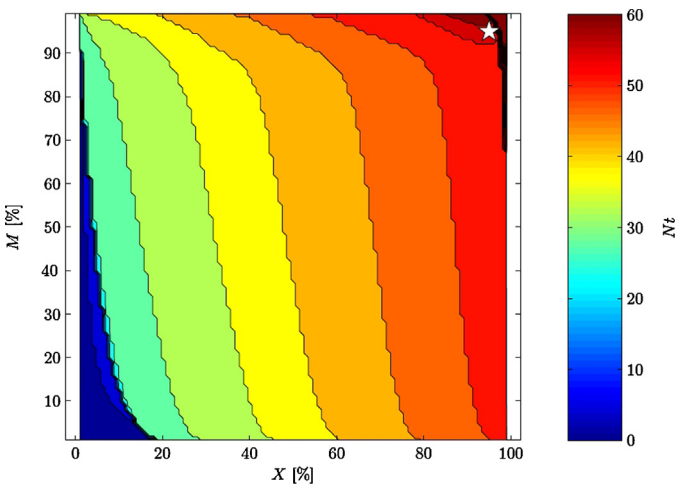
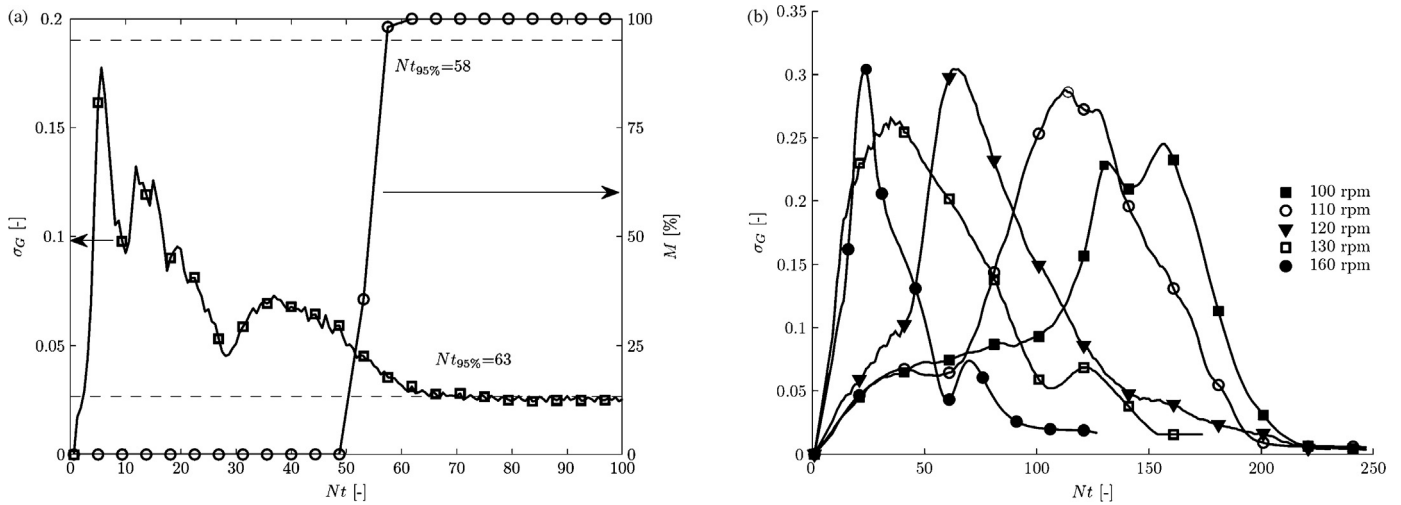


Fig. 4. Variation in time of the percentage of pixels mixed,  $M$ , against the local mixing threshold selected,  $X$ , for a Mobius® CellReady reactor, with a fill volume of 2 l agitated at 150 rpm ( $Re = 14,000$ ).



**Fig. 5.** (a) Variation in time of the percentage of mixed pixels,  $M$  ( $\square$ ), and of the standard deviation of the normalized green channel output,  $\sigma_G$  ( $\circ$ ); (b) variation in time of the standard deviation of the normalized green channel output,  $\sigma_G$ , for different orbital speeds. All data are for a cylindrical OSR with  $d_i = 10$  cm,  $d_o = 2.5$  cm.

must be exerted if meaningful comparisons between the results of different experiments and/or studies are to be made.

However, both approaches might prove useful for different purposes. The “cumulative” method employing  $M$  might be thought of as more reliable if the time when fully-mixed conditions are achieved is the main requirement, as it is not so sensitive to variations during the mixing process. On the other hand, the  $\sigma$  approach indicates variations in the mixing conditions during the process that could help reveal undesirable concentration gradients that, for instance, may be harmful to cells suspended in the reactor.

In relation to the latter, the  $\sigma_G$  methodology can help provide insights into the transient nature of the mixing process at different conditions and/or between different reactor geometries. A characteristic example is provided in Fig. 5(b), where the variation of  $\sigma_G$  with  $Nt$  in the 100 mm cylindrical bioreactor ( $h/d_i = 0.5$ ,  $d_o/d_i = 0.025$ ) is presented for five different speeds. It should be noted that for clarity only symbols corresponding to a few time instants are shown on each curve. All five curves indicate bell-shaped variations, but with notable differences: for the higher shaker table speeds, the curves have shapes akin to those of log-normal distributions, characterized by an initial rapid rise in

$\sigma_G$  followed by a long tail at higher  $Nt$  values; at lower speeds the peak is skewed towards the higher values of  $Nt$ , with a slow rise of  $\sigma$  during the initial stages of mixing, while the variation for 120 rpm is more symmetrical. The two types of curves may be thought of as characteristic of OSR mixing, those for high  $N$  being more akin to the rapid mixing process similar to that that might be expected in a stirred tank reactor, while those for low  $N$  indicate a more gradual dispersion and mixing in the reactor.

The colour indicated by a reaction such as the one utilized in the present work indicates a range of pH values, as mentioned in Section 2. It has been highlighted by Tan et al. [27] that what is indicated by the colour displayed in their single indicator experiments, is the transient time necessary for the entire fluid inside the flask to reach a certain pH threshold, which was not indicative of the mixing times necessary to achieve the final pH homogeneity.

To elucidate such effects, simultaneous measurements with the DISMT system and a pH probe were made both in the New Brunswick and in the CellReady STR bioreactors. Characteristic variations of  $\sigma_G$  obtained with the DISMT method and of the pH measured with a pH probe are presented in Fig. 6(a) and (b) for the New Brunswick and the CellReady, STR, respectively. The horizontal

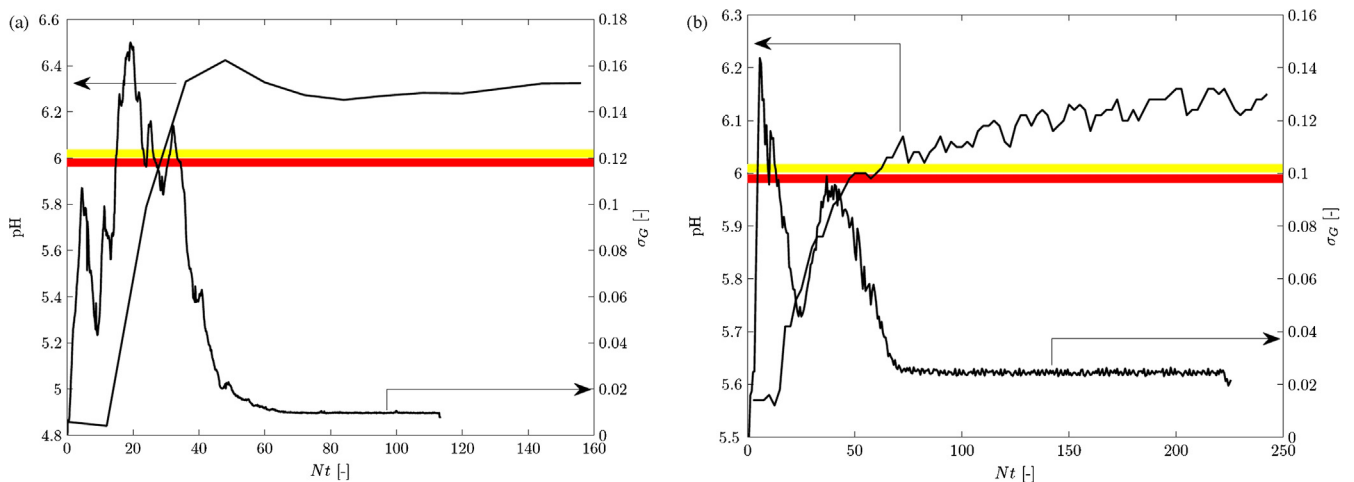


**Fig. 6.** Variation in time of the pH probe readings and of the standard deviation of the normalized green channel output,  $\sigma_G$ , for: (a) New Brunswick; and (b) CellReady Bioreactors (the horizontal lines indicate the pH threshold for the fluid to turn from red to yellow). (For interpretation of the references to colour in this figure legend, the reader is referred to the web version of this article.)

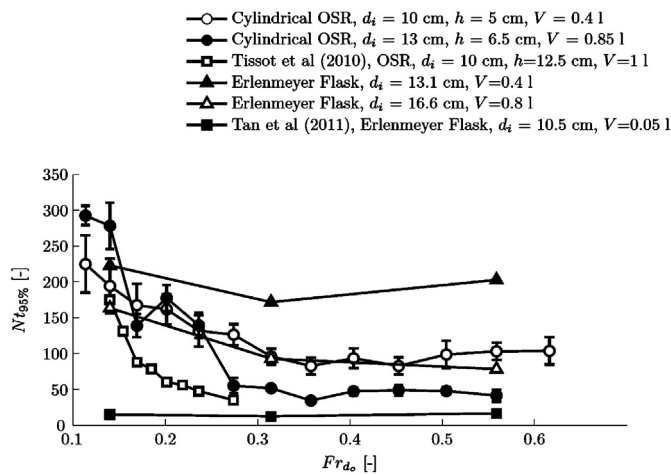


Fig. 7. Comparison of  $Nt_{95\%}$  versus  $Fr_{d_0}$  curves obtained in cylindrical and Erlenmeyer OSRs against those reported by Tissot et al. [26] and Tan et al. [27].

lines shown at pH 6 indicate the value for which the colour recorded with DISMT changes from yellow to red. The juxtaposition of the global (DISMT) with the local (pH probe) mixing results is made here solely to compare the qualitative trends indicated, not to consider quantitatively the level of mixing, as the local (probe) results are obviously not representative of the global state of mixing.

In both pH probe curves the level varies slightly even after the  $Nt$  value for which the DISMT result indicates that mixing has been completed. This may be due to a small drift in the pH probes' output that may be encountered with such devices. In addition, the

response time of pH probes is often limited, with readings being taken only every few seconds (1 s and 12 s for the CellReady and New Brunswick STR, respectively). The aforementioned limitations, single-point measurement and interference with the flow make pH probes built in a bioreactor suitable only for monitoring the pH during the entire duration of a bioprocess (which involves long times scales, often of one or more days), but not very effective when estimates of the relatively fast mixing dynamics (with time scales of minutes) are required in OSR applications. Clearly the colour technique is much better suited for OSR measurements, but the range of pH indicated by the reaction colours is finite and might affect the results obtained from visual inspection, whereas use of the  $\sigma_G$  values allows far more accurate determination of mixing times. It may be inferred from the comparison of the probe and  $\sigma_G$  DISMT data that they exhibit similar mixing times, for both the New Brunswick STR and CellReady cases. The effect that the finite band of pH indicated by the reaction colour may have on the accuracy of mixing time measurements with visual inspection methods has not been quantified to date.

A supplementary video (Supplementary-video.mov) is provided to show how the colour variation occurring in the bioreactor during the pH experiment is converted into a mixing time using the two methodologies previously outlined.

Supplementary material related to this article can be found, in the online version, at <http://dx.doi.org/10.1016/j.bej.2013.10.021>.

### 3.2. Mixing times and scaling in shaken bioreactors

The mixing time measurements obtained in this work are presented in this section and compared with previously reported data

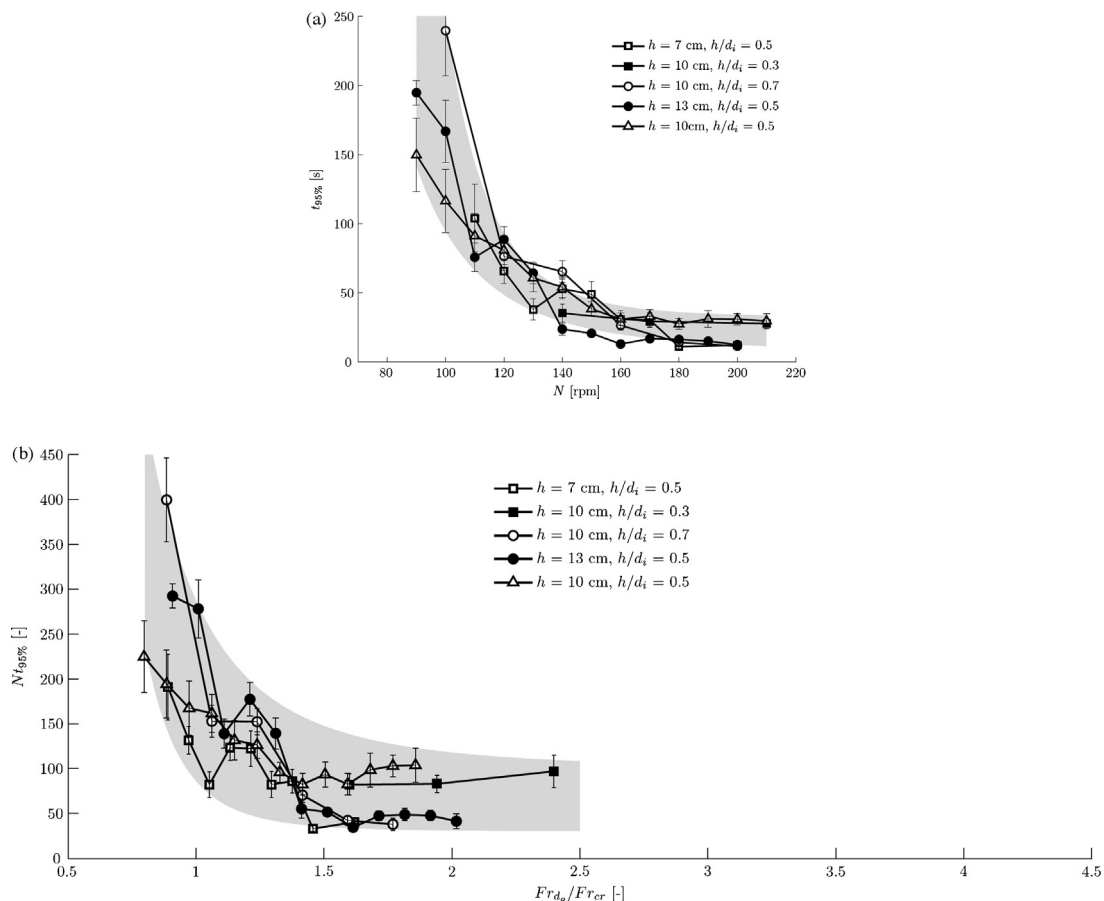
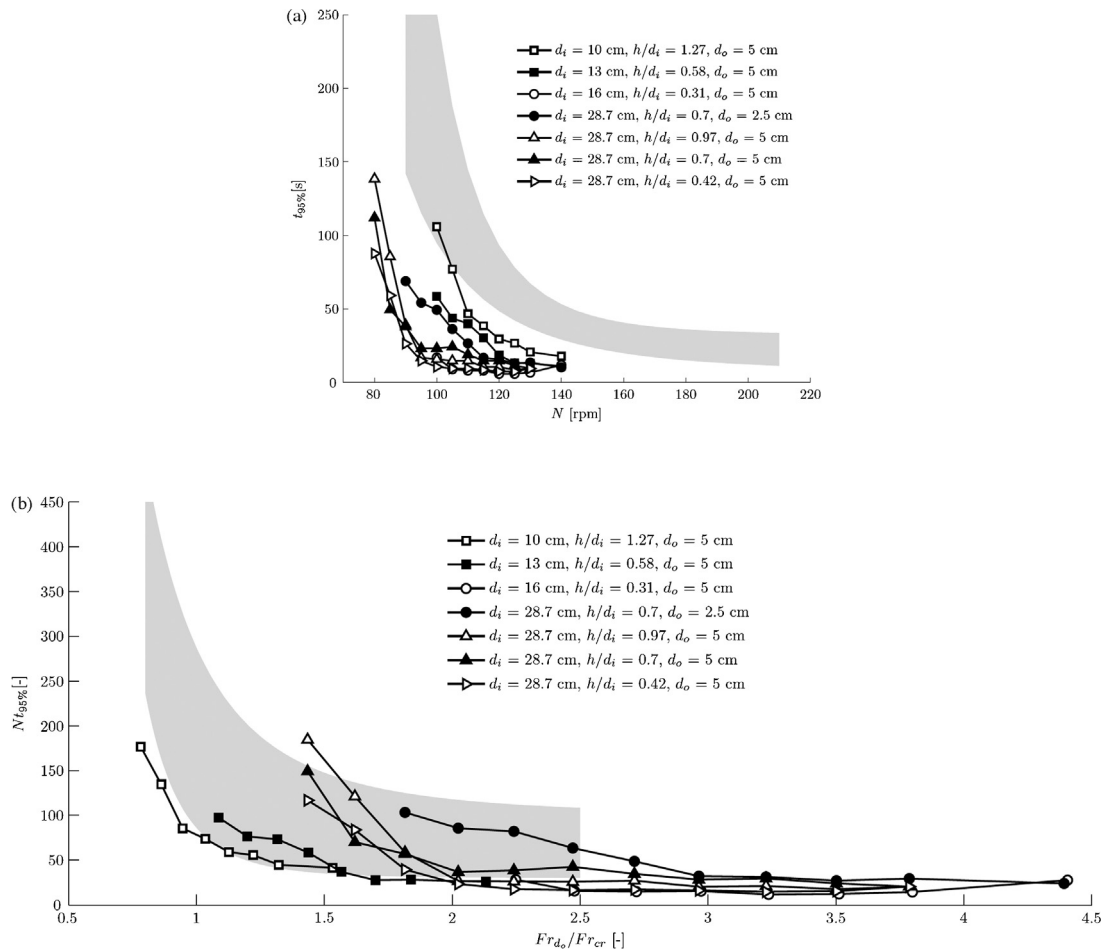


Fig. 8. (a) Variation of the mixing time with shaking speed and (b) Variation of the mixing number with  $Fr_{d_0}/Fr_{cr}$ , for cylindrical OSRs.



**Fig. 9.** Comparison of the present cylindrical OSR mixing data with those reported by Tissot et al. (2010), in terms of: (a) mixing time against speed (dimensional); (b) mixing number against the proposed scaling factor  $Fr_{d_0}/Fr_{cr}$  (non-dimensional).

obtained by Tissot et al. [26] in a cylindrical reactor and by Tan et al. [27] in Erlenmeyer flasks, in an effort to identify potential similarities and scaling between OSRs of different sizes, shaking speeds, filling volumes and/or shapes.

Mixing time measurements were obtained in the present work in the OSR and Erlenmeyer flask bioreactors over the ranges of experimental conditions listed in Table 1.

The variations of  $Nt_{95\%}$  values with  $Fr_{d_0}$  are presented in Fig. 7. It should be noted that  $Fr_{d_0} = 2\pi^2 N^2 d_0/g$  as mentioned in Section 2. Of course, comparisons must be made with care, not only due to the differences in geometry and operating conditions, but also due to the different techniques employed. For example, Refs. [26,27] determined the mixing time from visual observations, whereas for all the present experiments the DISMT data were processed using the methodology outlined in Section 2 and the image processing software described in detail by [29].

The mixing numbers for the 0.05l Erlenmeyer flask are much lower and cannot be readily compared with the rest. All other curves indicate that for  $Fr_{d_0}$  values less than around  $0.3Nt_{95\%}$  decreases with increasing  $Fr_{d_0}$ . For  $Fr_{d_0} > 0.3$  there is relatively little variation in  $Nt_{95\%}$ , except for the 0.4l Erlenmeyer flask. The data exhibit scatter, as might be expected due to the aforementioned differences in geometry, measurement technique etc. Furthermore, the presentation of mixing time data against  $Fr_{d_0}$  does not take into consideration the change in the flow regime in a shaken reactor from in-phase to out-of-phase flow, as the critical speed,  $N_{cr}$ , at which such a change takes place is not accounted for. The different flow regimes encountered for varying conditions point to the need

for a representation that can account for such changes and this is addressed later in this section.

In contrast, when only the cylindrical OSR data from the present work are considered, for which only the filling volume and reactor diameter were varied, even non-normalized results such as those presented in Fig. 8(a) indicate far more consistent trends. All the data indicate a similar variation, with the mixing time decreasing with shaking table speed from values of around 200 s at the low  $N$  range, tending nearly asymptotically to values of 20–30 s at speeds above 150 rpm. The range of variation of the data is indicated by the shaded area in the figure.

However, even for the present set of data, changes in flow regime will occur at different speeds when the filling volume, the orbital diameter or the reactor diameter is varied. An improved representation of the present data is shown in Fig. 8(b) where the same data as in Fig. 8(a) are plotted as variations of the mixing number  $Nt_{95\%}$  with the ratio  $Fr_{d_0}/Fr_{cr}$ , where the critical Froude number is estimated using the orbital diameter and the critical shaking speed obtained from either Eq. (3) or (4) depending whether condition  $h/d_i < (d_o/d_i)^{0.5}$  or  $h/d_i > (d_o/d_i)^{0.5}$  is satisfied. This representation helps to account for the different critical speeds encountered with different  $d_o/d_i$  and  $h/d_i$ , as the definition of  $N_{cr}$  takes into consideration both  $d_i$  and  $V_L$ , the volume of fluid in the reactor. The data in Fig. 8(b) show that, for the  $Fr$  range studied in this work, mixing numbers decrease with increasing  $Fr_{d_0}/Fr_{cr}$  up to 1.4 and remain approximately constant thereafter. Again, the range of variation of this set of data is indicated by a shaded area.

The potential of the proposed methodology for improved scaling protocols can be fully understood from Fig. 9(a) and (b), where the experimental data acquired in this work for shaken bioreactors of cylindrical geometry are directly compared against those collected by [26] for the same geometry, but for rather different operating conditions. In Fig. 9(a) a standard graph is made with dimensional axes ( $N$  versus  $t_{95\%}$ ). To improve the readability of the figure and reduce the clutter of curves, the data measured in this work are visualized by the grey shaded envelope. From Fig. 9(a) two main differences can be seen between the current data and those of [26]: (1) their data tend to reach a nearly constant mixing time at a lower speed; and (2) their constant mixing time is generally lower than the one found in this work. While the latter discrepancy can be justified by considering that in the two works a different methodology is used to determine the mixing time (visual versus post-processing analyses), the first one is more subtle and related to the onset of the flow transition reported by [23,29]. In the latter work it was shown that this flow transition is also related to the generation of turbulence, that enhances mixing. As mentioned before, this implies that the data of [26], which were generally obtained in larger tanks and for greater fluid height to cylinder diameter ratios, will undergo flow transition at very different speeds to those reported in the current work.

From this perspective a more universal representation might be achieved if the ratio  $Fr_{d_o}/Fr_{cr}$  is considered. This would help account for differences in orbital diameters between experiments, as well as reactor diameter and filling volume. A compilation of the current and the previously reported cylindrical OSR data by [26] is shown in Fig. 9(b), in terms of variation of the mixing number with  $Fr_{d_o}/Fr_{cr}$ . Similarly to Fig. 9(a), the data from the present work are shown as a range, indicated by the grey shaded area for  $Fr_{d_o}/Fr_{cr} < 2.4$ . Although differences should be expected for data from such a wide range of configurations and obtained in different laboratories, Fig. 9(b) clearly indicates the similarity of the variations of mixing number from different OSRs when considered against the normalized Froude number  $Fr_{d_o}/Fr_{cr}$ . The entire set of data in Fig. 9 indicates that the variation of  $Nt$  with  $Fr_{d_o}/Fr_{cr}$  may be represented by a power law relationship of the form

$$Nt = a \left( \frac{Fr_{d_o}}{Fr_{cr}} \right)^{-b} + c \quad (10)$$

Such a relation would represent most sets of data included in Fig. 9(b). The values of the factor  $a$  and of the exponent  $b$  might vary between different sets of data, to account for variations in the reactor size and operating parameters. At a sufficiently high  $Fr_{d_o}/Fr_{cr}$   $Nt = c$  and assumes a constant value of around 25–30. Eq. (10) at present offers a useful tool for the comparison of mixing time measurements in different cylindrical OSRs, and shows much promise for the development of a more universal scaling law for mixing in shaken bioreactors. At present, all the data included in Fig. 9(b) can be correlated with the power law of equation in the form  $Nt = 100.7(Fr_{d_o}/Fr_{cr})^{-1.245} + 25$ , albeit with a correlation coefficient of 0.56. However, it should be expected that if a robust measurement protocol is developed and widely adopted, formulation of a more universal scaling law should be possible to correlate all data obtained with this protocol, and differences in the  $a$  and  $b$  values for various OSR conditions might be minimized.

#### 4. Conclusions

In the present study the methodology of the DISMT technique for the measurement of mixing times in OSRs was assessed in detail. Various aspects of the data acquisition and processing procedures were considered and it was shown that utilization of the standard deviation  $\sigma_G$  of the green colour values recorded during an

experiment can help provide more reliable data that provide information not only on the final mixing time but also on the development of mixing during the process. It was pointed out that, in agreement with the DISMT work of [28] on STRs, care has to be exerted when selecting the fully-mixed criteria in an OSR.

DISMT measurements obtained in both a STR and an OSR were compared with simultaneously acquired pH probe data. The comparison indicated that the finite range of pH indicated by the colours displayed in the DISMT data can introduce uncertainties that should be further investigated in future.

The mixing time measurements obtained in cylindrical and Erlenmeyer shaken reactors for various operating conditions in the present work were compared with similar data previously reported in the literature. At low shaking table speeds the mixing number  $Nt$  decreases sharply with increasing speed and thereafter remains nearly constant. For some operating conditions mixing times as long as 100 s were obtained in orbitally shaken cylinders (see for example Fig. 8a and b), which may be related to the presence of inhomogeneity and local concentration gradients of pH and dissolved oxygen. These are extremely relevant in scaled up vessels, and for example the work of Serrato et al. [12] highlighted that cell growth, metabolism, and glycosylation pattern of an IgG1 monoclonal antibody were severely affected by the time spent by the cells in low DOT regions.

Differences between data obtained for various reactor diameters and filling volumes may be accounted for by considering the mixing time variation critical speed with  $N/N_{cr}$ , rather than simply  $N$ . This ratio accounts for the presence of in- or out-of-phase flow conditions in the OSR. When different reactor diameters, orbital diameters and other operating conditions are concerned, it was shown that consideration of the variation of mixing number with  $Fr/Fr_{cr}$  can aid scaling between mixing time measurements in different systems: all sets of data exhibited a trend that may be described by an equation of the form  $Nt = a(Fr/Fr_{cr})^{-b} + c$ .

This relation provides a most useful scaling law for mixing time determination in OSRs. The factor  $a$ , the exponent  $b$  and the constant  $c$  are configuration- and protocol-dependent, but it is expected that with a properly and widely implemented robust measurement protocol more universal scaling laws could be developed. This could be facilitated by a better understanding of the physics of the related flow and mixing processes and future work to elucidate further the mixing mechanisms in shaken bioreactors is called for. Nevertheless, the results of the present work show promise for the more reliable and accurate characterization of OSR mixing and research is on-going at present to extend the proposed scaling to a more wide range of fluid properties and operating conditions.

#### References

- [1] A.K. Pavlou, J.M. Reichert, Recombinant protein therapeutics – success rates, market trends and values to 2010, *Nat. Biotechnol.* 22 (2004) 1513–1519.
- [2] J.M. Reichert, C.J. Rosensweig, L.B. Faden, M.C. Dewitz, Monoclonal antibody successes in the clinic, *Nat. Biotechnol.* 23 (2005) 1073–1078.
- [3] Z. Doulgerakis, M. Yianneskis, A. Ducci, On the manifestation and nature of macroinstabilities in stirred vessels, *AIChE J.* 57 (2011) 2941–2954.
- [4] A. Ducci, Z. Doulgerakis, M. Yianneskis, Decomposition of flow structures in stirred reactors and implications for mixing enhancement, *Ind. Eng. Chem. Res.* 47 (2008) 3664–3676.
- [5] R. Escudie, A. Line, Experimental analysis of hydrodynamics in a radially agitated tank, *AIChE J.* 49 (2003) 585–603.
- [6] M. Yianneskis, Z. Popiolek, J.H. Whitelaw, An experimental study of the steady and unsteady flow characteristics of stirred reactors, *J. Fluid Mech.* 175 (1987) 537–555.
- [7] T.A. Bibila, C.S. Ranucci, K. Glazomitsky, B.C. Buckland, J.G. Aunins, Monoclonal-antibody process-development using medium concentrates, *Biotechnol. Prog.* 10 (1994) 87–96.
- [8] M. Schroder, K. Matischak, P. Friedl, Serum- and protein-free media formulations for the Chinese hamster ovary cell line DUKXB11, *J. Biotechnol.* 108 (2004) 279–292.

- [9] S.S. Ozturk, Engineering challenges in high density cell culture systems, *Cytotechnology* 22 (1996) 3–16.
- [10] A.R. Lara, E. Galindo, O.T. Ramirez, L.A. Palomares, Living with heterogeneities in bioreactors, *Mol. Biotechnol.* 34 (2006) 355–381.
- [11] A.W. Nienow, C. Langheinrich, N.C. Stevenson, A.N. Emery, T.M. Clayton, N.K.H. Slater, Homogenisation and oxygen transfer rates in large agitated and sparged animal cell bioreactors: some implications for growth and production, *Cytotechnology* 22 (1996) 87–94.
- [12] J.A. Serrato, L.A. Palomares, A. Meneses-Acosta, O.T. Ramirez, Heterogeneous conditions in dissolved oxygen affect N-glycosylation but not productivity of a monoclonal antibody in hybridoma cultures, *Biotechnol. Bioeng.* 88 (2004) 176–188.
- [13] A.W. Nienow, Reactor engineering in large scale animal cell culture, *Cytotechnology* 50 (2006) 9–33.
- [14] A.W. Nienow, W.H. Scott, C.J. Hewitt, C.R. Thomas, G. Lewise, A. Amanullah, R. Kiss, S.J. Meieer, Scale-down studies for assessing the different stress parameters on growth and product quality during animal cell culture, *Chemical Engineering Research and Design* (2013), <http://dx.doi.org/10.1016/j.cherd.2013.04.002>.
- [15] C.Y. Sargent, G.Y. Berquig, M.A. Kinney, L.A. Hiatt, R.L. Carpenedo, R.E. Berson, T.C. McDevitt, Hydrodynamic modulation of embryonic stem cell differentiation by rotary orbital suspension culture, *Biotechnol. Bioeng.* 105 (2010) 611–626.
- [16] J.A. King, W.M. Miller, Bioreactor development for stem cell expansion and controlled differentiation, *Curr. Opin. Chem. Biol.* 11 (2007) 394–398.
- [17] T. Anderlei, C. Cesana, C. Burki, M. De Jesus, M. Kuhner, F. Wurm, R. Lohser, Shaken bioreactors provide culture alternative, *Gen. Eng. Biotechnol. News* 1st of November 2009 (2009) 44.
- [18] C.M. Liu, L.N. Hong, Development of a shaking bioreactor system for animal cell cultures, *Biochem. Eng. J.* 7 (2001) 121–125.
- [19] W. Klöckner, J. Büchs, Advances in shaking technologies, *Trends Biotechnol.* 30 (2012) 307.
- [20] J. Gardner, G. Tatterson, Characterization of mixing in shaker table containers, *Biotechnol. Bioeng.* 39 (1992) 794–797.
- [21] J. Büchs, U. Maier, C. Milbradt, B. Zoels, Power consumption in shaking flasks on rotary shaking machines: II. Nondimensional description of specific power consumption and flow regimes in unbaffled flasks at elevated liquid viscosity, *Biotechnol. Bioeng.* 68 (2000) 594–601.
- [22] W. Klöckner, S. Tissot, F. Wurm, J. Büchs, Power input correlation to characterize the hydrodynamics of cylindrical orbitally shaken bioreactors, *Biochem. Eng. J.* 65 (2012) 63–69.
- [23] W. Weheliye, M. Yianneskis, A. Ducci, On the fluid dynamics of shaken bioreactors – flow characterisation and transition, *AIChE J.* 59 (2013) 334–344.
- [24] J. Büchs, S. Lotter, C. Milbradt, Out-of-phase operating conditions, a hitherto unknown phenomenon in shaking bioreactors, *Biochem. Eng. J.* 7 (2001) 135–141.
- [25] U. Maier, J. Büchs, Characterisation of the gas–liquid mass transfer in shaking bioreactors, *Biochem. Eng. J.* 7 (2001) 99–106.
- [26] S. Tissot, M. Farhat, D.L. Hacker, T. Anderlei, M. Kuhner, C. Comninellis, F. Wurm, Determination of a scale-up factor from mixing time studies in orbitally shaken bioreactors, *Biochem. Eng. J.* 52 (2010) 181–186.
- [27] R.K. Tan, W. Eberhard, J. Büchs, Measurement and characterization of mixing time in shake flasks, *Chem. Eng. Sci.* 66 (2011) 440–447.
- [28] F. Cabaret, S. Bonnot, L. Fradette, P.A. Tanguy, Mixing time analysis using colorimetric methods and image processing, *Ind. Eng. Chem. Res.* 46 (2007) 5032–5042.
- [29] G. Rodriguez, W. Weheliye, T. Anderlei, M. Micheletti, M. Yianneskis, A. Ducci, Mixing time and kinetic energy measurements in a shaken cylindrical bioreactor, *Chem. Eng. Res. Des.* (2013), <http://dx.doi.org/10.1016/j.cherd.2013.1003.1005>.
- [30] A. Ducci, M. Yianneskis, Vortex identification methodology for feed insertion guidance in fluid mixing processes, *Trans. IChemE Chem. Eng. Res. Des.* 85 (2007) 543–550.
- [31] A. Ducci, M. Yianneskis, Vortex tracking and mixing enhancement in stirred processes, *AIChE J.* 53 (2007) 305–315.
- [32] S.C. Kaiser, R. Eibl, D. Eibl, Engineering characteristics of a single-use stirred bioreactor at bench-scale: the Mobius CellReady 3L bioreactor as a case study, *Eng. Life Sci.* 11 (2011) 359–368.
- [33] L.A. Melton, C.W. Lipp, R.W. Spradling, K.A. Paulson, DISMT—determination of mixing time through color changes, *Chem. Eng. Commun.* 189 (2002) 322–338.
- [34] K.C. Lee, M. Yianneskis, A liquid crystal thermographic technique for the measurement of mixing characteristics in stirred vessels, *Chem. Eng. Res. Des.* 75 (1997) 746–754.
- [35] M. Micheletti, L. Nikiforaki, K.C. Lee, M. Yianneskis, Particle concentration and mixing characteristics of moderate-to-dense solid–liquid suspensions, *Ind. Eng. Chem. Res.* 42 (2003) 6236–6249.